Enhancement of photoluminescence intensity of erbium doped silica containing Ge nanocrystals: distance dependent interactions

IOP Publishing Nanotechnology
Nanotechnology **26** (2015) 045202 (11pp) doi:10.1088/0957-4484/26/4/045202

Enhancement of photoluminescence intensity of erbium doped silica containing Ge nanocrystals: distance dependent interactions

S Manna[1], R Aluguri[1], R Bar[1], S Das[1,3], N Prtljaga[2,4], L Pavesi[2] and S K Ray[1]

[1] Department of Physics, Indian Institute of Technology Kharagpur, Kharagpur-721 302, India
[2] Dipartimento di Fisica, Laboratorio di Nanoscienze, Università di Trento, Via Sommarive 14, I-38100 Povo (Trento), Italy

E-mail: physkr@phy.iitkgp.ernet.in

Received 21 September 2014, revised 24 November 2014
Accepted for publication 2 December 2014
Published 6 January 2015

Abstract

Photo-physical processes in Er-doped silica glass matrix containing Ge nanocrystals prepared by the sol–gel method are presented in this article. Strong photoluminescence at 1.54 μm, important for fiber optics telecommunication systems, is observed from the different sol–gel derived glasses at room temperature. We demonstrate that Ge nanocrystals act as strong sensitizers for Er^{3+} ions emission and the effective Er excitation cross section increases by almost four orders of magnitude with respect to the one without Ge nanocrystals. Rate equations are considered to demonstrate the sensitization of erbium luminescence by Ge nanocrystals. Analyzing the erbium effective excitation cross section, extracted from the flux dependent rise and decay times, a Dexter type of short range energy transfer from a Ge nanocrystal to erbium ion is established.

Keywords: Ge nanocrystal, Er sensitization, 1.54 μm photoluminescence emission

(Some figures may appear in colour only in the online journal)

1. Introduction

Modern fiber-optics communication systems use near infrared light at 1.54 μm wavelength, which coincides with minimum transmission loss of silica fibers. A rare earth element, especially erbium, is useful for optical signal amplification in fibers because of their ~1.54 μm emission owing to the intra-4*f* transition from the first excited to the ground state ($^4I_{13/2} \rightarrow {}^4I_{15/2}$) [1]. It has been reported that the Er ions' luminescence may be enhanced by introducing Si nanocrystals (Si NCs) into the host matrix favouring the energy transfer from silicon NCs to the Er^{3+} ions [2]. Enhancement of more than four orders of magnitude of the effective excitation cross section up to 10^{-6}–10^{-17} cm^2 in Er doped SiO_2 containing Si NCs has been found [3, 4]. In comparison, Er in SiO_2 has a cross section of $\sim 10^{-21}$ cm^2. Hence, Er doped SiO_2 containing Si NCs has been studied extensively by researchers [5–17]. Since Ge, the other important Group IV element, has larger excitonic Bohr radius (~26 nm) compared to Si (~5 nm) leading to stronger quantum confinement, it might be a potential alternative material as a sensitizer for Er^{3+} ions. Additionally, the tunability of size dependent emission from sol–gel derived Ge NCs [18], and the possible improvement of the pumping efficiency due to the close value of the Ge exciton energy with the 1.54 μm transition from Er^{3+} ions motivate the use of Ge NCs as sensitizers for Er^{3+} ions. However, there are only a few reports showing the enhancement of Er photoluminescence (PL) in presence of Ge NCs [19–24]. In particular, Ge related oxygen deficiency centers (GeODCs) form at the interface of Ge NC and SiO_2. Kanjilal *et al* [25, 26] have shown that energy transfer from

[3] Currently at Centre for Applied Research in Electronics (CARE), IIT Delhi, India.
[4] Currently at LDSD group, University of Sheffield, Sheffield, S3 7RH, UK.

Table 1. Size, photoluminescence peak and full width at half maximum (FWHM) for different Ge nanocrystals containing sol–gel samples.

Sample name	Amount of Ge (%)	Annealing temperature (°C)	Annealing time	Size from HRTEM (nm)	Band gap energy (E_g) from PL (eV)	FWHM of the PL emission band (eV)
7.5% Ge_a750 °C	7.5	750	2 h 30 min	4.1 ± 0.8	1.32	0.31
7.5% Ge_a850 °C	7.5	850	2 h 30 min	5.0 ± 1.0	1.25	0.32
10% Ge_a750 °C	10	750	2 h 30 min	6.1 ± 1.0	1.23	0.34
10% Ge_a850 °C	10	850	2 h 30 min	6.8 ± 1.5	1.19	0.33

GeODCs to the Er^{3+} ions occurs for photons with energy larger than 3.07 eV.

In this paper, we study the role of Ge NCs as sensitizers of Er^{3+} ions. Er^{3+} induced PL has been observed at room temperature along with Ge NC emission for energies larger than the Ge band gap. The characteristics of the Er induced PL emission using resonant and non-resonant excitation are discussed. Particular care has been paid to use photon energies lower than 3 eV in order to avoid direct excitation of GeODCs. We have studied the Er emission related rise and decay to have the idea of effective excitation cross section of Er and consequently to investigate the energy transfer mechanism from Ge NCs to Er^{3+}, which was not studied so far.

2. Experimental details

Tetraethyl ortho-silicate and erbium tetrachloride ($ErCl_3$, $6H_2O$) were chosen as the starting materials to prepare Er-doped SiO_2 glasses by sol–gel process. With a view to growing Ge NCs within the SiO_2 matrix, $GeCl_4$ was incorporated in the reaction [22]. The 'sol' was kept for a few days within enclosed polystyrene containers for aging till a stiff 'gel' was formed. These gels were dried at room temperature for 30 days followed by the sintering in air ambient at 100–500 °C for 5 h. Three types of sol–gel glasses were prepared, one containing only Ge, a second doped with only Er, and a third one co-doped with Er and Ge. Finally, the samples were annealed in the presence of a $N_2 + H_2$ gas mixture (9:1 ratio) at different temperatures ranging from 700 to 850 °C for 2.5 h to induce the nucleation of Ge NCs by reduction of GeO_2. In this respect, the mechanism of Ge NCs formation can be discussed in a nutshell. Precipitation of metallic Ge occurs due to the reduction of Ge ions with different oxide states in the presence of H_2 within the silica matrix. Since Si^{4+} is much more stable compared to Ge^{4+}, there is no effect on Si^{4+} due to the annealing.

High-resolution transmission electron microscopic (HRTEM) images of Ge NCs were taken using a JEOL 2010 microscope operated at 200 kV. The microstructural properties of the grown samples were analyzed by x-ray diffraction using a Phillips X'Pert PRO MRD x-ray diffractometer. To record the optical transmission spectra of the glasses, a Perkin Elmer Lambda 45 UV/visible spectrometer was used. PL characteristics of sol–gel glasses were studied using 532 and 980 nm laser sources, a monochromator and liquid nitrogen cooled InGaAs detector. Lifetime of the 1.54 μm emission peak was measured by using the 532 nm laser excitation with a mechanical chopper and lock-in amplifier. Low temperature PL measurements were done using a closed cycle cryostat.

3. Structural properties

3.1. Size of nanocrystals

Ge NCs of different sizes have been grown by using different Ge fractions and by varying the annealing temperature (see table 1). TEM micrographs of Ge NCs are shown in figures 1(a)–(d) for a glass with 7.5% Ge content annealed at 750 °C and 850 °C, and for a glass with 10% Ge content annealed at 750 °C and 850 °C, respectively. The selected area electron diffraction patterns corresponding to the 7.5% Ge annealed at 750 °C is found to be ring-like, few characteristic directions in the diffraction pattern are indexed to be the (111), (220) and (311) crystallographic planes of a cubic Ge and GeO_2 phases. These findings have been further supported by x-ray diffraction measurements reported in the following. Lattice fringes of such Ge NCs could be observed in figure 1(f) confirming the formation of crystalline Ge. Figures 1(a)–(d) show that the sizes of NCs are changed by varying the Ge content as well as the annealing temperature.

Analysis of several TEM images allows to yield the average diameters of nucleated Ge NCs (table 1) and their size distributions. The average Ge NC diameter increases with Ge content and annealing temperature. This is due to the increased precipitation of Ge atoms, which are incorporated in the NCs samples. The average NC density has been derived by counting the number of NCs within an image area L^2. If N is the resulting number, and assuming an uniform dispersion of NCs, the NC density results to be $N^{3/2}/L^3$. Typically, the NCs density for a 10% Ge annealed at 850 °C glass is found to be $(7.8 \pm 0.5) \times 10^{16}$ cm^{-3}.

3.2. X-ray diffraction of Ge nanocrystals

X-ray diffraction measurements yield the crystallite characteristics. Figure 2 presents the diffraction pattern for 10% Ge annealed at different temperatures. As-prepared as well as 700 °C annealed samples do not show any diffraction peak indicating the growth of amorphous Ge in the SiO_2 matrix. Samples annealed at temperatures higher than 700 °C show the formation of NCs from amorphous Ge clusters. For 750

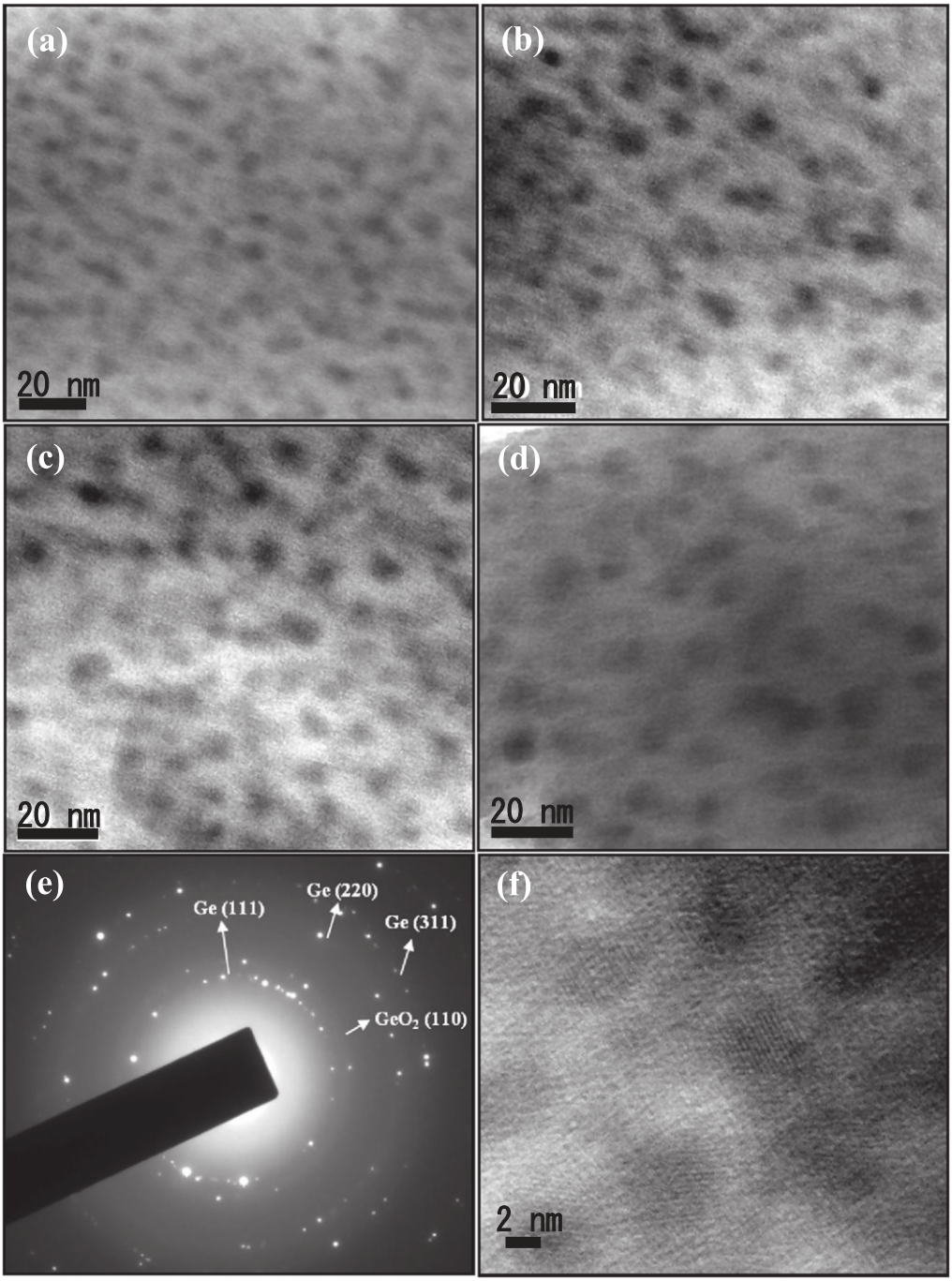

Figure 1. TEM images of Ge NCs in silica matrix for (a) 7.5% Ge annealed at 750 °C (b) 7.5% Ge annealed at 850 °C (c) 10% Ge annealed at 750 °C and (d) 10% Ge annealed at 850 °C; (e) Selected area electron diffraction pattern of 7.5% Ge annealed at 750 °C sample showing a ring pattern. Specific directions are indexed as cubic Ge (111), (220) and (311) planes along with the GeO_2 (110). Lattice fringes of few Ge nanocrystals could be seen in (f) for this 7.5% Ge annealed at 750 °C sample.

and 850 °C annealed samples, clear diffraction peaks corresponding to the crystallographic (111), (220) and (311) planes of the cubic Ge phase are observed at 27.20°, 45.17° and 53.59°, respectively. For higher temperatures, the broadening of the peak decreases due to the increased crystallinity. For the 850 °C annealed sample, a weak crystallographic (111) peak of hexagonal GeO_2 is also observed in the diffraction pattern.

4. Optical properties

4.1. Absorption and PL characteristics

Absorption spectra of the sol–gel samples show both the NC absorption as well as the characteristic intra 4*f*–4*f* absorption of Er^{3+} ions. Figure 3 compares the absorption of an Er doped glass with the one of Ge NC and Er co-doped glass. The absorption of the Er doped glass shows the characteristic

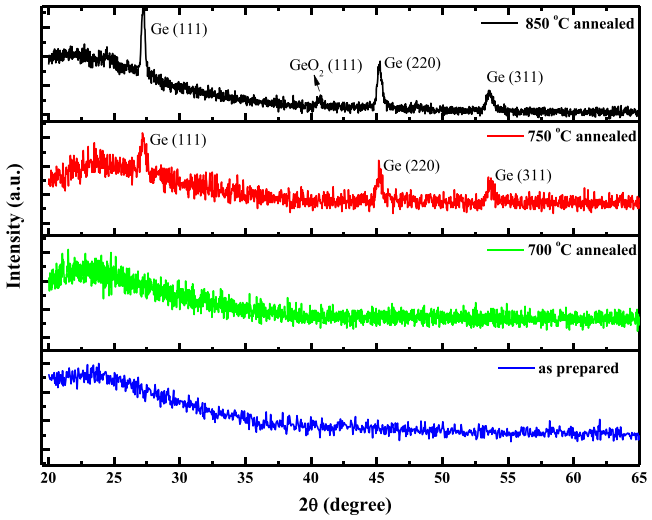

Figure 2. X-ray diffraction spectra of Er doped SiO_2 glasses containing Ge NCs (10% Ge) at different annealing temperatures of 700, 750 and 850 °C along with the as-prepared one.

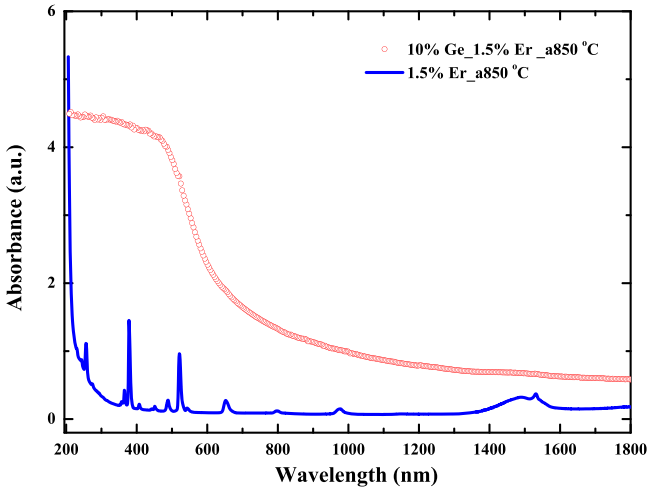

Figure 3. Absorbance spectra related to Er doped glasses with and without Ge NCs for 1.5% Er annealed at 850 °C and 10% Ge, 1.5% Er annealed at 850 °C samples.

peaks at 376, 488, 521, 648, 800, 976, 1480 and 1540 nm. With addition of Ge NCs in the Er doped glass, the absorption increases owing to the absorption of Ge NCs. As an example we show in figure 3 the absorption of a 10% Ge content glass with 1.5% of Er and annealed at 850 °C. From this comparison, it is clear that the Ge NC dominates the absorption at 532 nm. Therefore, the 532 nm laser line can be used as the non-resonant line to Er for its optical pumping.

Figure 4 shows the PL emission from Ge NCs, embedded within SiO_2 matrix, using a 532 nm laser. The PL peak position red shifts with the increase of Ge amount and/or the annealing temperature from 750 °C to 850 °C. For example, the PL peak is at 937 nm (1.32 eV) for the 7.5% Ge annealed at 750 °C glass, whereas it is red shifted to 1038 nm (1.19 eV) for 10% Ge annealed at 850 °C glass. This is attributed to the increase in the size of the Ge NCs, confirmed by TEM. The emission peak position for this kind of sol–gel derived Ge NC

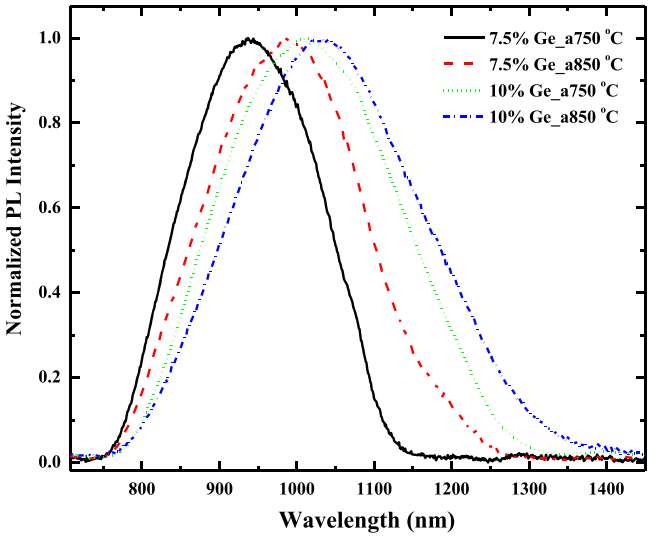

Figure 4. Photoluminescence spectra for Ge NCs embedded SiO_2 samples using 532 nm laser excitation. PL peak position is red shifted with increase in Ge amount from 7.5% to 10%. PL peak is also red shifted with increase in annealing temperature from 750 °C to 850 °C for both 7.5% and 10% Ge content sample.

appears to be systematically at longer wavelengths than for Ge NC obtained by vapor deposition [27]. Ruddy *et al* [18] have observed the same trend for solution processed Ge NCs in the wavelength range 860–1230 nm. Full-width-at-half-maximum (FWHM) of the PL emission has also been measured at low temperature (10 K, not shown), but there is no considerable narrowing of the peak width, indicating the presence of inhomogeneous broadening [28]. The emission peak is broadened by the distribution of sizes of Ge NCs to a FWHM of 300–350 meV, as observed in figure 4.

To get Er induced PL emission, we have used 980 nm and 532 nm pumps. The 980 nm excitation line is resonant with the $^4I_{11/2}$ level of Er^{3+} ions, whereas 532 nm is non-resonant. Figure 5(a) shows that with the increase in annealing temperature, the PL intensity increases. When the glass is co-doped with Ge NCs, the PL intensity increases even further, which is due to the sensitization of Er^{3+} ions by Ge NCs. It also shows that the enhancement in the integrated PL intensity is 1.8 times larger for the 850 °C annealed sample as compared to that annealed at 750 °C. Varying Er concentrations upto 1.5% yields an increase of the integrated PL intensity by a factor of 5.5 for the Er doped glass and 2.2 for the Er and Ge NCs co-doped glass, as shown in the figure 5(b). The enhancement is attributed to the increase in the number of optically active Er^{3+} ions in the matrix. Figure 5(c) presents the Er related PL spectra due to the indirect pumping of Er ions using 532 nm laser for different temperature and Er concentrations and trends are the same as when exciting by 980 nm laser.

Afterwards, all the measurements and calculations will be done corresponding to the 532 nm excitation. Measurements corresponding to the 980 nm pump can be used to calculate the number of only directly excited Er^{3+} ions since 980 nm

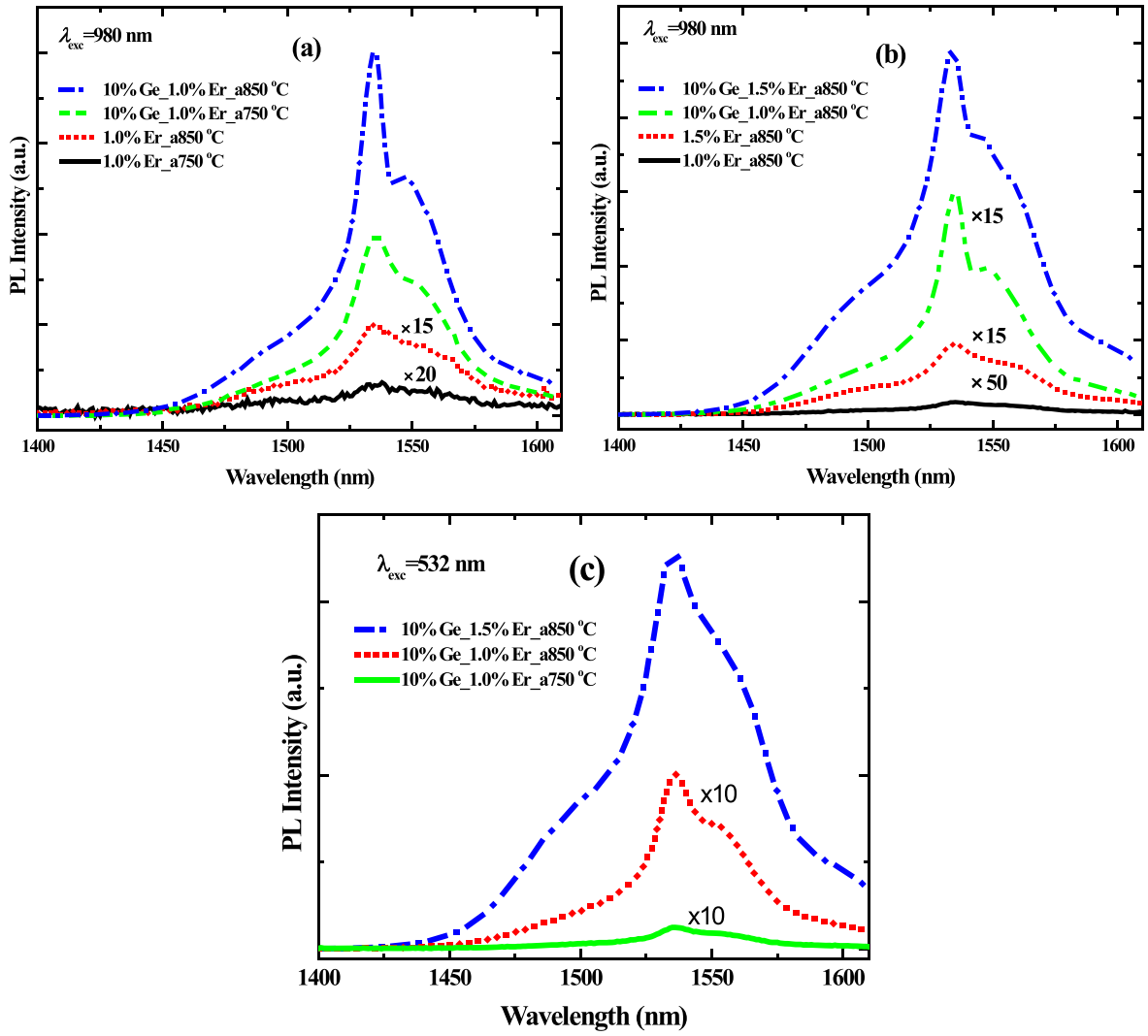

Figure 5. (a) Photoluminescence spectra for silica glass with and without Ge NCs for (a) different annealing temperatures (750 and 850 °C) upon excitation by a 980 nm laser and (b) different Er concentrations upon excitation by a 980 nm laser and (c) photoluminescence spectra for silica glass with Ge NCs for different anneal temperatures and Er concentrations upon excitation by a 532 nm laser.

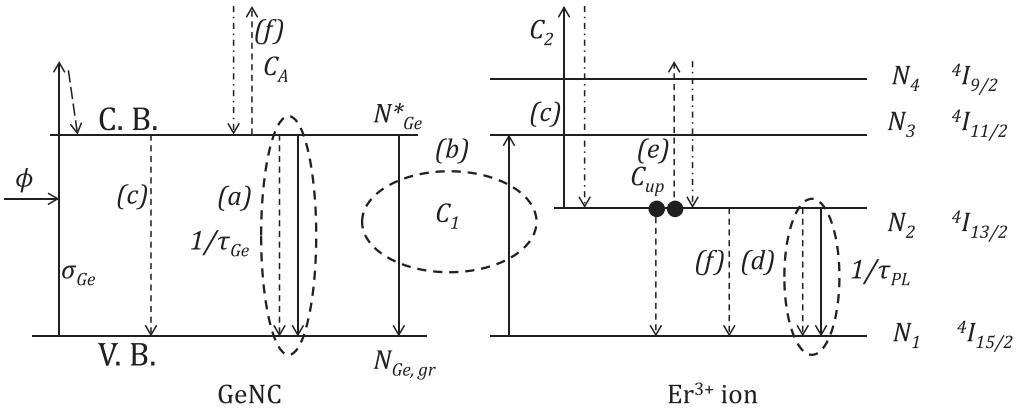

Figure 6. A model of the energy transfer from Ge NCs to Er^{3+} ions. The different symbols and transitions are described in the text.

will be able to excite Er ions both directly as well as indirectly via Ge NCs.

4.2. Emission mechanism

A model of the the interaction between Ge NCs and Er^{3+} ions can be derived by using rate equations. Details of the model for the system of Si NC sensitizing Er ions can be found in [7, 13]. Interaction between Ge NC and Er^{3+} ions is schematically presented in figure 6, where different excitations and de-excitation pathways for the Ge NC and Er ions are considered. Ge NC is modeled as a two level system with two band edge levels. It should be noted that since we have got the Ge NC direct PL peak in the energy region 1.20–1.32 eV, we assume that the $^4I_{11/2}$ level of Er^{3+} ion (1.26 eV) is resonant with the Ge NC conduction band edge. The excitation of Ge NC by an incident photon flux ϕ is modeled through an effective excitation cross section, σ_{Ge}, which yields a rate of exciton generation $\sigma_{Ge}\phi$. Excited Ge NCs can decay to the ground state radiatively or non-radiatively with a total recombination lifetime of τ_{Ge} (transitions marked as (a) in figure 6). On the other hand, Ge NC couple to Er^{3+} ions, and transfer the excitation energy to Er which gets excited in the $^4I_{11/2}$ level as shown in the process marked (b) in figure 6. The coupling coefficient is labeled C_1. The excited Er^{3+} ions then might also be further excited to higher excited states by direct absorption of the exciton recombination energy from Ge NCs. This process is known as excited-state absorption (ESA), which is marked as (c) in figure 6 and the corresponding ESA coefficient is labeled C_2. Excited Er^{3+} ions then can radiatively or nonradiatively relax from the $^4I_{13/2}$ to the ground $^4I_{15/2}$ state with a total recombination lifetime τ_{PL} (process marked as (d) in figure 6). Another recombination channel is the co-operative up conversion (CUC) which is a de-excitation process resulting from the interaction between two excited Er^{3+} ions; one of the ions relaxes to the ground state giving the excess energy to the other ion which gets excited to higher energy state (process marked as (e) in figure 6). C_{up} is the co-operative up-conversion coefficient. Another de-excitation path of Er ions from the $^4I_{13/2}$ level is via the Auger excitation of excitons (AEEs) in the Ge NC. The process is modeled by the Auger coefficient C_A and is described by process (f) in figure 6. From this model the following rate equations are derived:

$$\frac{dN^*_{Ge}}{dt} = \sigma_{Ge}\phi N_{Ge,gr} - \frac{N^*_{Ge}}{\tau_{Ge}} - C_1 N_1 N^*_{Ge} - C_2 N_2 N^*_{Ge}, \quad (1)$$

where N^*_{Ge} is the density of excited Ge NCs, while $N_{Ge,gr}$ is the density of Ge NC in the ground state. Here $N_{Ge} = N^*_{Ge} + N_{Ge,gr}$ is the total density of Ge NCs in the sample, N_1 and N_2 are the density of Er ions in the ground and in the first excited state $^4I_{13/2}$ respectively.

The density N_2 of the first excited Er state is given by:

$$\frac{dN_2}{dt} = C_1 N_1 N^*_{Ge} - \frac{N_2}{\tau_{PL}} - C_{up} N_2^2 - C_A N_2 N^*_{Ge}. \quad (2)$$

Here we assume a very fast relaxation from all higher levels to $^4I_{13/2}$. From equation (2) we can define the effective Er excitation cross section σ_{eff} as

$$\sigma_{eff}\phi = C_1 N^*_{Ge}. \quad (3)$$

Finally, it holds that $N_c = N_1 + N_2$, where N_c is the density of Er coupled to Ge NC.

Assuming a steady state condition, i.e. CW excitation, we get N^*_{Ge} and then

$$\sigma_{eff} = \frac{C_1 N_{Ge,gr}\sigma_{Ge}}{C_1 N_1 + C_2 N_2 + \sigma_{Ge}\phi + \dfrac{1}{\tau_{Ge}}}. \quad (4)$$

Assuming a low excitation flux regime, equation (2) becomes

$$\frac{dN_2}{dt} = \sigma_{eff}\phi N_1 - \frac{N_2}{\tau_{PL}} \quad (5)$$

since for low fluxes, the effect of de-excitation processes like CUC, ESA and AEE are negligible. Then in steady state condition and using $N_1 = N_c - N_2$ we get

$$N_2 = \frac{N_c \phi \sigma_{eff}\tau_{PL}}{1 + \phi\sigma_{eff}\tau_{PL}}. \quad (6)$$

To calculate the absolute values of N_2, we have measured the power dependent PL intensity of all the samples and deduced the number of excited Er ions by a quantitative comparison of the emitted photon flux with a reference Er doped glass supplied by Corning [3, 12]. To find the maximum value of N_2, equation (6) is not properly valid because CUC, ESA and AEE effects have to be considered also.

Figure 7 shows the dependence of calculated N_2 values with photon flux (for both 980 and 532 nm pump) and the ratio N_2/N_{Er} (excited Er fraction) for 532 nm for the 10% Ge, 1.5% Er sample annealed at 850 °C. It is noticed that the amount of indirectly excited Er^{3+} ion has a trend for saturation's. Therefore, although the exact value of $N_2(max)$ is not

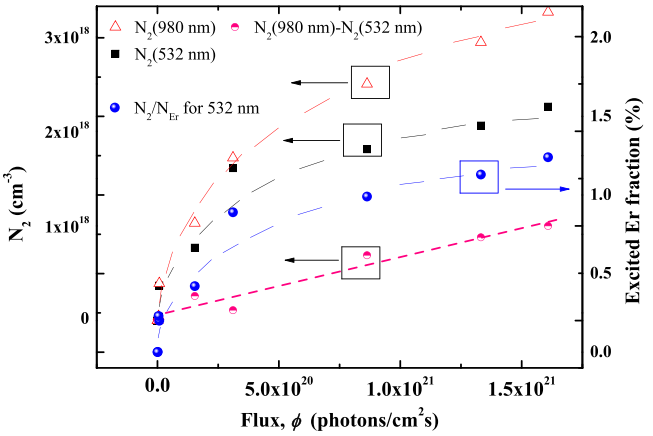

Figure 7. Excited Er^{3+} ions density (N_2) as a function of the 980 nm (both direct + indirect excitation) and 532 nm (only indirect excitation) photon flux for 10% Ge, 1.5% Er annealed (850 °C) sample. The difference provides only directly excited Er^{3+} ions density. Indirectly excited fraction of Er^{3+} ions as a function of the 532 nm photon flux is also shown. All the dashed lines are guide to the eye.

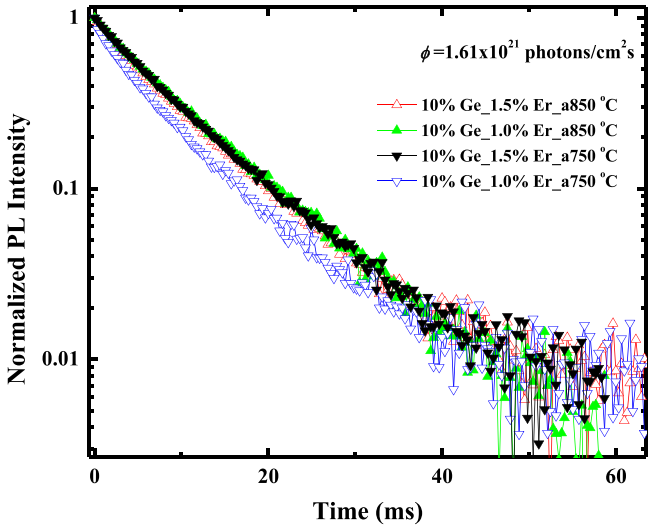

Figure 8. Decay profiles corresponding to the 1.54 μm emission for different samples using a 532 nm pump photon flux of 1.61×10^{21} photons cm^{-2} s^{-1}.

known, we can presume that the experimental value of N_2 at the highest pump flux of 1.61×10^{21} photons cm^{-2} s^{-1} is close to $N_2(max)$. This premise is useful for approximate calculation of some parameters related to the Er^{3+} excitation dynamics. Our calculation shows that for a particular amount of Er, the density of indirectly excited Er becomes more for 850 °C compared to 750 °C annealed samples (tabulated in table 2). The maximum density of indirectly excited Er, $N_2(max)$, obtained is 2.26×10^{18} cm^{-3} for the best performing sample (above one). The corresponding maximum Er fraction, $N_2(max)/N_{Er}$ is 1.23%, whereas for Si NCs, several groups have reported different maximum excitable Er fraction up to 5% [3, 8, 29–31]. The possible outcome of the small number of ions coupled to nanocrystals is the low fraction of nonresonantly excitable erbium ions compared to the optical transparency limit (inversion of 50% Er ions, i.e., $N_2/N_{Er} = 50\%$), ultimately limiting to achieve very high optical efficiency in structures alike Si NCs based system.

Considering that the fraction of Er^{3+} ions excited through Ge NC is the same for both 532 and 980 nm pumps, the subtraction of the density of excited Er ions ($N_2[980] - N_2[532]$) in figure 7 provides the contribution of directly excited Er^{3+} ions to the 1.54 μm PL intensity. We have observed that the number of directly excited Er ions does not show the saturation behavior, indicating the direct excitation of Er^{3+} ions is still significantly possible by the resonant 980 nm pump.

4.3. PL lifetime

A very important parameter in the model is τ_{PL}. Time resolved decay measurements of the Er emission are shown in figure 8. The decay line shape is a stretched exponential, which results from the superposition of single exponential functions with a distribution $\rho(\tau)$, where τ is the decay time constant of each single exponential. In this case, the PL intensity is given by [12]

$$I(t) = I_0 \exp\left\{-\left(\frac{t}{\langle\tau\rangle}\right)^{\beta}\right\} = \int_0^{\infty} I_0 \exp\left\{-\left(\frac{t}{\tau}\right)\right\}\rho(\tau)\mathrm{d}\tau \quad (7)$$

and the mean relaxation time $\langle\tau\rangle$ is

$$\langle\tau\rangle = \frac{\tau}{\beta}\Gamma(1/\beta), \quad (8)$$

where β is a non-exponential exponent, Γ is the Gamma function and $\langle\tau\rangle = \tau_{PL}$ is the average PL life time. By using relations (7) and (8), τ_{PL} have been extracted from the PL decay line shapes for different Ge and Er contents and different annealing temperatures. The long measured lifetime shows that the matrix is almost defect free. Indeed, increasing the annealing temperature, the lifetime increases. On the other hand, we also observe that on increasing the Er content in the film, the lifetime increases, which indicates that we are far from the critical concentration where Er clustering is observed. Another interesting trend is the fact that the lifetime shortens as the photon flux increases (as can be seen from figure 9(a)). This suggests that de-excitation processes like CUC effect are important in these sol–gel glasses. CUC becomes a key factor when Er concentration or photon flux is high or both are high. We can take into account the up-conversion effect by adding an additional term to the rate equation (5) for Er–Er ion pair interactions in the excited state

$$\frac{\mathrm{d}N_2}{\mathrm{d}t} = \sigma_{\mathrm{eff}} N_1 \phi - \frac{N_2}{\tau_2} - C_{\mathrm{up}} N_2^2. \quad (9)$$

For $\phi = 0$ (pump is off), equation (9) becomes

$$\frac{\mathrm{d}N_2}{\mathrm{d}t} = -\frac{N_2}{\tau_2} - C_{\mathrm{up}} N_2^2, \quad (10)$$

where C_{up} is the up-conversion coefficient.

Instead of calculating the exact analytical form of the total decay time τ_{PL} we consider a simplified form as:

$$\frac{1}{\tau_{\mathrm{PL}}} \simeq \frac{1}{\tau_2} + C_{\mathrm{up}} N_2 \quad (11)$$

which is nothing but a linear dependence of $1/\tau_{\mathrm{PL}}$ on N_2. τ_{PL} as a function of flux and as well as $1/\tau_{\mathrm{PL}}$ as a function of N_2 are shown in figures 9(a) and (b), respectively, for different samples. The CUC coefficients C_{up} extracted from linear fits are $(7.0 \pm 5.0) \times 10^{-17}$, $(2.0 \pm 1.0) \times 10^{-17}$ and $(1.5 \pm 0.1) \times 10^{-17}$ cm^3 s^{-1} for glasses containing 1.5% Er annealed at 750 °C, 1% Er annealed at 850 °C and 1.5% Er annealed at 850 °C, respectively. The conclusion can be drawn from the above fact that the CUC coefficients decrease with annealing temperature, which has also been observed in the case of Si NC–Er system [3]. This signifies that the pump flux required to achieve transparency limit will be appreciably enhanced in the presence of CUC effect.

Table 2. Density of Er^{3+} ions present in the samples, the maximum excitable Er^{3+} ions, its ratio to the total Er^{3+} ions.

Amount of Ge (%)	Annealing temperature (°C)	Amount of Er (%)	N_{Er} ($\times 10^{20}$ cm^{-3})	$N_{2,\,max}$ ($\times 10^{18}$ cm^{-3})	$N_{2,\,max}/N_{Er}$ (%)	1.54 μm PL decay time, τ_{PL} (ms)[a]
10	750	1	1.22	0.20	0.16	6.65
10	850	1	1.22	1.31	1.07	8.65
10	750	1.5	1.83	0.68	0.37	8.36
10	850	1.5	1.83	2.26	1.23	8.07

[a] At $\phi = 1.6 \times 10^{21}$ photons cm^{-2} s^{-1}.

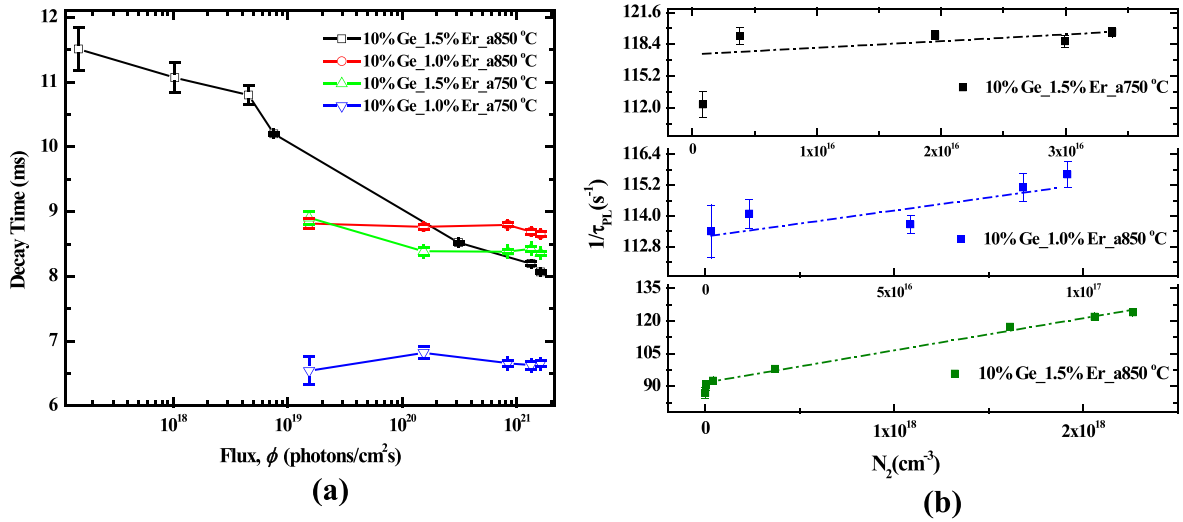

Figure 9. (a) Photoluminescence decay lifetime of samples with different annealing temperatures and Er content plotted as a function of the 532 nm pump photon flux and (b) plot of $1/\tau_{PL}$ as a function of N_2 (532 nm excitation) for different samples to find the up-conversion coefficients.

The photon flux for transparency becomes after calculation:

$$\phi_{1/2} = \begin{cases} \dfrac{1}{\sigma_{\text{eff}}\tau_2} \text{without up-conversion,} & (12) \\ \dfrac{1}{\sigma_{\text{eff}}\tau_2}\left(\dfrac{1}{2}C_{\text{up}}N_{\text{Er}}\tau_2 + 1\right) \text{with up-conversion.} & (13) \end{cases}$$

It can be found that the photon flux which for a glass with 10% Ge content, 1.5% Er content and annealed at 850 °C and by using the parameters ($\sigma_{eff} = 4 \times 10^{-17}$ cm^2, $\tau_2 = 10.9$ ms, $N_{Er} = 1.83 \times 10^{20}$ cm^{-3}) is $\phi_{1/2} \sim 2.3 \times 10^{18}$ photons cm^{-2} s^{-1} without up-conversion and $\sim 4 \times 10^{19}$ photons cm^{-2} s^{-1} with up-conversion. If we consider the effect of ESA, $\phi_{1/2}$ increases even further. However, experimentally, transparency does not appear when the system is excited by a flux equal to the above calculated flux. This is because the amount of optically active Er^{3+} ions is a fraction of the total Er^{3+} ions.

Previously, we have discussed the decay time of Er^{3+} ions from $^4I_{13/2}$ to $^4I_{15/2}$ state. Not only the decay time, but also the rise time from the ground state to the $^4I_{13/2}$ state is important for the study of the decay dynamics of Er^{3+} ions. As the laser beam is switched on, Er population in the first excited level will increase with time up to saturation with a characteristic time of τ_{rise}. The increase of the excited Er^{3+} ion population can be written as [32]:

$$N_2(t) = \frac{N_c\phi\sigma_{\text{eff}}\tau_{\text{PL}}}{1 + \phi\sigma_{\text{eff}}\tau_{\text{PL}}}\left[1 - \text{e}^{-\left(\phi\sigma_{\text{eff}} + \frac{1}{\tau_{\text{PL}}}\right)t}\right], \quad (14)$$

where

$$\frac{1}{\tau_{\text{rise}}} = \left(\sigma_{\text{eff}}\phi + \frac{1}{\tau_{\text{PL}}}\right). \quad (15)$$

With increasing pump power, the increase of the PL intensity becomes faster and faster. Moreover, by using equation (15), one can calculate σ_{eff}. It should be noted that the PL rise line-shape has a typical stretched exponential dependence which looks like

$$I(t) = I_0\left[1 - \exp\left\{-\left(\frac{t}{\tau_{\text{rise}}}\right)^{\beta}\right\}\right]. \quad (16)$$

By measuring the time dependence of the PL emission under pulsed excitations, the PL rise time (τ_{rise}) for Er ions within silica matrix with or without Ge NCs pumped at 532 nm for different pump fluxes has been calculated. For the 10% Ge content, 1% Er content and 850 °C annealing temperature sample, the values of β are plotted in figure 10. β decreases with the increase of photon flux which indicates that the rise and decay line shapes are almost single exponential at low pump power and become stretched exponential

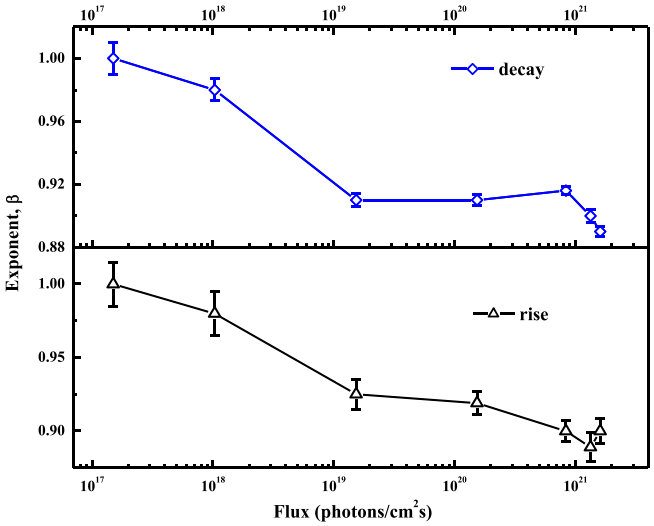

Figure 10. Extracted values of β as a function of the pumping flux for both PL rise and decay.

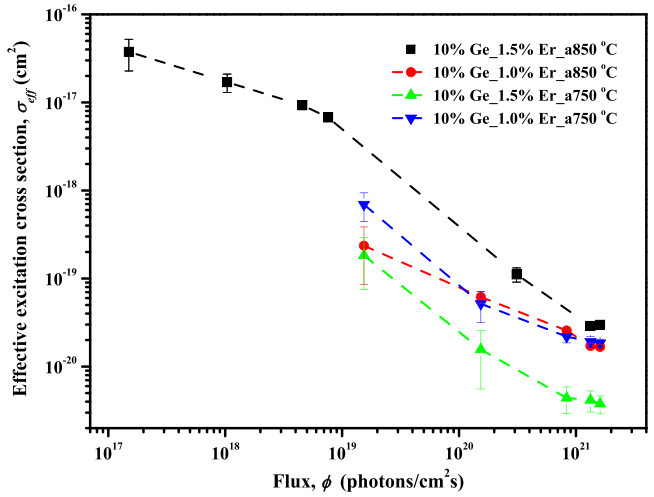

Figure 11. Calculated values of σ_{eff} as a function of the 532 nm pump flux plotted for different samples.

at high pump powers. $\beta \neq 1$ indicates a distribution of recombination paths that in our case are associated with the onset of co-operative effects, such as CUC or ESA, at high photon fluxes.

4.4. Flux dependent Er-excitation cross section

From the rise and decay lifetimes, we calculated σ_{eff}, which is reported in figure 11, as a function of 532 nm pump flux for different samples. The best performing sample is found to be 10% Ge content, 1.5% Er content and 850 °C annealing temperature one. For this sample, σ_{eff} is found to be $(4 \pm 1) \times 10^{-17}$ cm^2 at a photon flux of 1.5×10^{17} photons cm^{-2} s^{-1}. The presence of Ge NCs enhances the effective excitation cross section for Er luminescence by almost four orders of magnitude relative to the Er doped

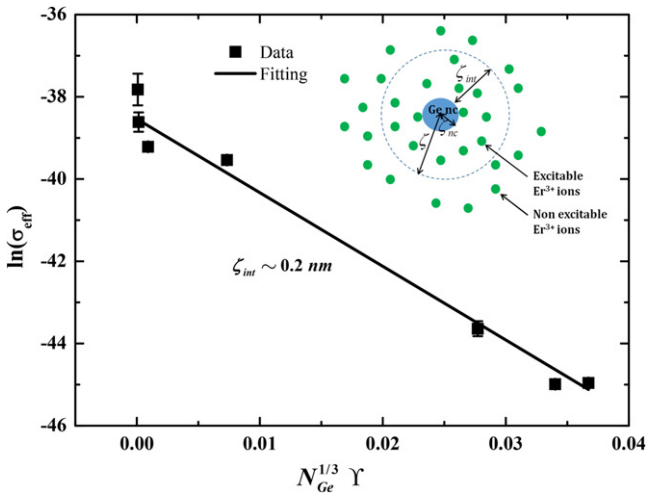

Figure 12. Dependence of the effective excitation cross section as a function of the interaction radius, indicating the presence of a Dexter kind of energy transfer mechanism. Inset shows the schematic diagram of the system which shows interaction region between a Ge NC and Er^{3+} ions.

SiO_2 without any Ge NCs. The large absorption cross section of Ge NCs is responsible for this enhanced effective excitation cross section. σ_{eff} for Er coupled to Si NC is larger than the values here reported by one order of magnitude [3]. At moderate photon fluxes of 1.5×10^{19} cm^{-2} s^{-1}, σ_{eff} decreases to $(3 \pm 1) \times 10^{-19}$ cm^2. The decrease of σ_{eff} with an increase of the photon flux is similar to what was observed for the Er–Si NC system [3]. From equation (3), we can write: $\sigma_{\text{eff}} = C_1 N^*_{\text{Ge}}/\phi$. For low or moderate photon flux, N^*_{Ge} is likely to increase linearly with flux. The decrease of σ_{eff} in figure 11 is thus attributed to the pump flux-dependent C_1 value. It implies that the coupling constant between Er and Ge NC falls rapidly with an increase of the pump photon flux. According to [3], we interpret this as an indication of a distance dependent interaction between Ge NCs and Er^{3+} ions.

4.5. Distance dependent interaction between Ge NC and Er^{3+} ions

We can define an effective volume Γ_{eff} containing the excited Er ions around each Ge NC. Beyond this volume the Er ions remain unexcited. A schematic diagram of this model is presented in the inset of figure 12. In this scheme, the density of Er ions (N_2), which are excited by the Ge nanocrystals, is the product of the density of Er ions in the matrix, the density of Ge nanocrystals (N_{Ge}) and the interaction volume (Γ_{eff}):

$$N_2 = N_{\text{Ge}} N_{\text{Er}} \Gamma_{\text{eff}} = N_{\text{Ge}} N_{\text{Er}} \frac{4}{3} \pi \left(\zeta^3 - {\zeta_{\text{nc}}}^3 \right)$$

here ζ and ζ_{nc} are the radii of the interaction sphere and the

Ge NC, respectively.Then

$$N_{Ge}\zeta^3 = N_{Ge}\zeta_{nc}{}^3 + \frac{3}{4\pi}\frac{N_2}{N_{Er}},$$

$$\Rightarrow N_{Ge}{}^{1/3}\zeta = \sqrt[3]{N_{Ge}\zeta_{nc}{}^3 + \frac{3}{4\pi}\frac{N_2}{N_{Er}}},$$

$$\Rightarrow N_{Ge}{}^{1/3}\Upsilon = \sqrt[3]{N_{Ge}\zeta_{nc}{}^3 + \frac{3}{4\pi}\frac{N_2}{N_{Er}}} - N_{Ge}{}^{1/3}\zeta_{nc}, \quad (17)$$

where $\Upsilon = (\zeta - \zeta_{nc})$ is the interaction distance.

Since all the quantities on the rhs of the equation (17) are known, plotting σ_{eff} as a function of $N_{Ge}{}^{1/3}\Upsilon$ yields information on the nature of the Ge NC–Er interaction. For the above calculation, the average radius and density of Ge NCs have been taken as 3.4 nm and 7.8×10^{16} cm^{-3} (from the HRTEM measurement), respectively.

Figure 12 shows the plot of σ_{eff} as a function of the calculated values of $N_{Ge}{}^{1/3}\Upsilon$. It is better fitted with an exponential decay behavior ($e^{-\Upsilon}$) compared to the power law dependence (Υ^{-6}) of Förster energy transfer. From the exponential fit of $\sigma_{eff} = \sigma_0 \exp(-N_{Ge}{}^{1/3}\Upsilon/\Xi)$, values of σ_0, and Ξ are extracted to be 1.8×10^{-17} cm^2 and 0.006, respectively. Now putting $\sigma_{eff}/\sigma_0 = e^{-1}$, and $\Upsilon = \zeta_{int}$, we get $\zeta_{int} = \Xi N_{Ge}{}^{-1/3}$, which gives $\zeta_{int} \sim 0.2$ nm. So, we have found that a distance dependent Dexter like interaction with an average interaction distance of ~0.2 nm can model the interaction between a Ge NC and Er^{3+} ions. The interaction distance found for Si NC and Er is 0.4 nm [3], which explains the larger σ_{eff} for Si NC–Er than for Ge NC–Er. Our findings clearly show the role of Ge NCs in the sensitization scheme, where they are able to excite very efficiently Er ions in close proximity to their surface, but not efficient away from the surface, which in turn decreases the number of ions coupled to NCs. That is why this distance dependent interaction becomes a limitation for a reasonable population of Er ions in the first excited state to achieve transparency limit.

4.6. Temperature dependent PL spectra

Finally, we have carried out the temperature dependent measurement of the PL signal around 1.54 μm for our best performing sample (1.5% Er 10% Ge 850 °C annealed one). Figure 13 shows the PL spectra for different temperatures from 10 K towards the room temperature. It has been observed that for the above measured range, there is no considerable quenching of integrated PL intensity, whereas for only Er doped SiO_2, temperature dependent quenching takes place (not shown). This is because of the fact that the nonradiative quenching processes are suppressed for silica matrix containing Ge NCs compared to that without NCs. Also from the figure 13, we got the nice interesting fact that instead of decrease in integrated PL intensity with increase in temperature of the sample, it becomes more or less same; rather, it is distributed around the 1.54 μm within the region of 1.44 μm–1.7 μm. This is basically nothing but the excitation of Er ions, due to thermal redistribution (inset of figure 13), from below 1.54 μm to the higher energy levels

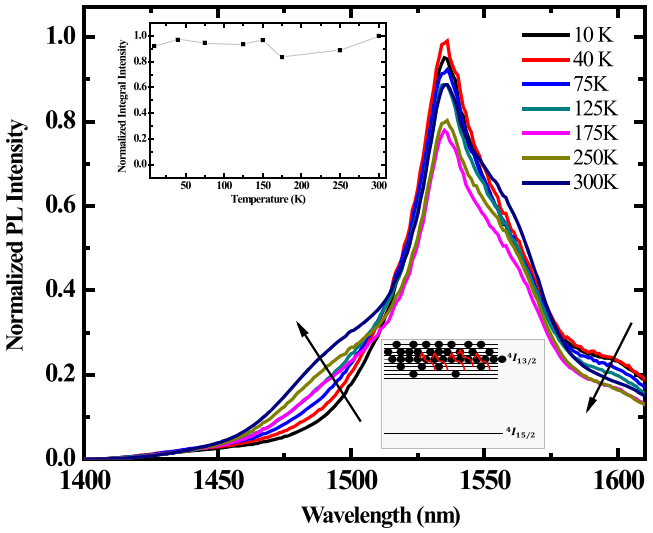

Figure 13. Temperature dependent PL spectra of Er doped SiO_2 glass with Ge NCs. Inset shows the integrated PL intensity as a function of temperature and thermal redistribution within the $^4I_{13/2}$ levels.

created due to the stark splitting. The above unquenched Er emission also confirms the negligible presence of non-radiative trap centers as also corroborated by the large decay time (>8 ms) of Er emission. This indicates the possible further optimization of Ge nanocrystal sensitization scheme for the very high optical efficiency fabricating the samples using CMOS compatible techniques.

5. Conclusions

Room temperature PL in the third telecommunication window (1.54 μm) from Er^{3+} ions has been reported. It has been shown that in presence of Ge NCs, the effective excitation cross section of Er^{3+} ion is enhanced by almost four orders of magnitude from $\sim10^{-21}$ cm^{-3} to $\sim10^{-17}$ cm^{-3}. This is ascribed to the energy transfer from Ge NCs to Er^{3+} ions. Our measurements shows that maximum 1.23% of total Er^{3+} ions could be indirectly excited by Ge NCs at a high pumping photon flux of 1.6×10^{21} cm^{-2} s^{-1}. We modeled the Ge NC–Er interaction as a Dexter interaction which occurs with a characteristic interaction distance of ~0.2 nm. Dexter type energy transfer was confirmed from the exponential dependence of the effective excitation cross section of Er with the inter-distance between a Ge NC and Er ion. We also quantified the characteristic parameters for de-excitation phenomenon like co-operative up-conversion. However, the integrated Er PL intensity being temperature independent, corresponding to the sample of maximum excitable fraction, shows the huge suppression of non-radiative trap states. As a whole this work gives a range of parameters suitable to model the Er–Ge NC systems in order to optimize the material for all optical amplifiers.

Acknowledgments

This work is financially supported by the DST-ITPAR project on Nanophotonics.

References

[1] Polman A 1997 *J. Appl. Phys.* **82** 1
[2] Kenyon A J, Trwoga P F, Federighi M and Pitt C W 1994 *J. Phys.: Condens. Matter* **6** L319
[3] Garrido B, García C, Seo S-Y, Pellegrino P, Navarro-Urrios D, Daldosso N, Pavesi L, Gourbilleau F and Rizk R 2007 *Phys. Rev.* B **76** 245308
[4] Fujii M, Yoshida M, Kanzawa Y, Hayashi S and Yamamoto K 1997 *Appl. Phys. Lett.* **71** 1198
[5] Kik P G, Brongersma M L and Polman A 2000 *Appl. Phys. Lett.* **76** 2325
[6] Franzó G, Bonitelli S, Pacifici D, Priolo F, Iacona F and Bongiorno C 2003 *Appl. Phys. Lett.* **82** 3871
[7] Pacifici D, Franzó G, Priolo F, Iacona F and Negro L D 2003 *Phys. Rev.* B **67** 245301
[8] Wojdak M, Klik M, Forcales M, Gusev O B, Gregorkiewicz T, Pacifici D, Franzò G, Priolo F and Iacona F 2004 *Phys. Rev.* B **69** 233315
[9] Daldosso N *et al* 2005 *Appl. Phys. Lett.* **86** 261103
[10] Lebour Y, Pellegrino P, García C, Moreno J A and Garrido B 2006 *J. Appl. Phys.* **100** 073103
[11] Daldosso N, Navarro-Urrios D, Melchiorri M, Pavesi L, Sada C, Gourbilleau F and Rizk R 2006 *Appl. Phys. Lett.* **88** 161901
[12] Navarro-Urrios D *et al* 2009 *J. Appl. Phys.* **106** 093107
[13] Savchyn O, Todi R M, Coffey K R and Kik P G 2010 *Opt. Mater.* **32** 1274
[14] Walters R J, Bourianoff G I and Atwater H A 2005 *Nat. Mater.* **4** 143
[15] Sychugov I, Elfström N, Hallén A, Linnros J and Qiu M 2007 *Opt. Lett.* **32** 1878
[16] Izeddin I, Timmerman D, Gregorkiewicz T, Moskalenko A S, Prokofiev A A, Yassievich I N and Fujii M 2008 *Phy. Rev.* B **78** 035327
[17] Han H-S, Seo S-Y and Shin J H 2001 *Appl. Phys. Lett.* **79** 4568
[18] Ruddy D A, Johnson J C, Smith E R and Neale N R 2010 *ACS Nano* **4** 7459
[19] Sánchez J M, Serna R, Toudert J, Alén B and Ballesteros C 2014 *Opt. Lett.* **39** 4691
[20] Heng C L, Finstad T G, Storås P, Li Y J, Gunnæs A E and Nilsen O 2004 *Appl. Phys. Lett.* **85** 4475
[21] Jensen J S, Pedersen T P L, Chevallier J, Nielsen B B and Larsen A N 2006 *Nanotechnology* **17** 2621
[22] Das K, Nagarajan V, NandaGoswami M L, Panda D, Dhar A and Ray S K 2007 *Nanotechnology* **18** 095704
[23] Guzman J *et al* 2009 *Appl. Phys. Lett.* **95** 201904
[24] Aluguri R, Das S, Manna S, Singha R K and Ray S K 2012 *Opt. Mater.* **34** 1430
[25] Kanjilal A, Tsushima S, Götz C, Rebohle L, Voelskow M, Skorupa W and Helm M 2009 *J. Appl. Phys.* **106** 063112
[26] Kanjilal A, Rebohle L, Voelskow M, Skorupa W and Helm M 2009 *J. Appl. Phys.* **106** 026104
[27] Ray S K, Maikap S, Banerjee W and Das S 2013 *J. Phys. D: Appl. Phys.* **46** 153001
[28] Takeoka S, Fujii M and Hayashi S 2000 *Phys. Rev.* B **62** 16820
[29] Oton C J, Loh W H and Kenyon A J 2006 *Appl. Phys. Lett.* **89** 031116
[30] Garrido B, García C, Pellegrino P, Navarro-Urrios D, Daldosso N, Pavesi L, Gourbilleau F and Rizk R 2006 *Appl. Phys. Lett.* **89** 163103
[31] Navarro-Urrios D, Daldosso N, García C, Pellegrino P, Garrido B, Gourbilleau F, Rizk R and Pavesi L 2007 *Japan. J. Appl. Phys.* 1 **46** 6626
[32] Priolo F, Franzo G, Iacona F, Pacifici D and Vinciguerra V 2001 *Mater. Sci. Eng.* B **81** 9